A&A 478, 889–895 (2008)
DOI: 10.1051/0004-6361:20078419

Astronomy & Astrophysics

Collisionless transport of energetic electrons in the solar corona at current-free double layers

K. W. Lee[1,2], J. Büchner[1], and N. Elkina[1,3]

[1] Max-Planck-Institut für Sonnensystemforschung, Germany
e-mail: lee@mps.mpg.de
[2] Institute of Space Science, NCU, Taiwan
[3] Keldysh Institute for Applied Mathematics, Russia

Received 4 August 2007 / Accepted 9 November 2007

ABSTRACT

Context. Impinging electron beams in the solar chromosphere generate hard X-ray radiation (HXR) through the collisional Bremstrahlung thick target model. The deduced electron distributions usually exhibit a broken-power-law. Assuming that the initial distribution function was a drift-Maxwellian, this indicates that the distribution of energetic electrons changes in the course of their propagation, from the looptop acceleration site to the high density chromosphere, via a collisionless scattering mechanism.
Aims. The formation of a broken-power-law spectrum via the particle interaction with the current-free weak double layers (DLs) in a reverse current beam plasma system.
Methods. The unstable waves generated in current-free coronal plasmas are first studied by means of a linear instability analysis. For most probable coronal plasma parameters, a one-dimensional electrostatic Vlasov-code simulation is performed to understand the nonlinear evolution of the instabilities and their influences on the electron distribution.
Results. DL structures cause a dissipation of low energy beam electrons and a stagnation of return-current electrons. Fast electron holes are formed, a secondary two-stream instability, caused by the DL-accelerated electrons. Electron and ion heating by DLs also takes place.
Conclusions. The plasma distributions of energetic electrons in the solar corona evolve via their interactions with nonlinear large-amplitude phase-space structures. At the late stage of evolution, the low-energy electrons are slowed down while the high energy part stays uninfluenced after the appearance of DLs. A major part of the return-current electrons change their direction to that of the injected beam. As a result the distribution becomes a broken-power-law as observed by chromospheric HXR radiation.

Key words. plasmas – waves – Sun: corona – Sun: flares

1. Introduction

The forward-fitting of hard X-ray (HXR) observations provides number of energetic electrons and the instantaneous electron flux of solar flares (Aschwanden et al. 1999). The HXR emission from a flare can be characterized by its location either as coronal or as chromospheric. The coronal emission provides relatively low energy photons (≤30 keV). Its characteristics are consistent with a hot quasi-thermal plasma radiation. The chromospheric "footpoint" emission, on the other hand, is thought to be generated by a vast number of non-thermal particles accelerated during a flare (Fletcher 2005).

The electron spectra, deduced from the HXR observations, exhibit different power-law indices at the footpoints and in the upper corona. The footpoint X-ray fluxes, obtained by HXIS/SMM in a range of 16–30 keV (MacKinnon 1985), were found to be only 15−28% of the fluxes obtained by extrapolating the same energy range from HXRBS/SMM spectra at higher energies of 25–300 keV (Zharkova 1997). These results indicate that electron dissipation must occur during the propagation, especially of the lower energy electrons, while the higher energy part of the electron spectrum stays approximately unchanged.

In a fully ionized plasma, a magnetic field is induced by the injected energetic electron-beam. According to Faraday's induction law, the magnetic field flux is maintained as a constant in a perfectly-conducting environment. Hence, a backward propagating electron-beam is therefore generated by the induced electromotive force to cancel the flux change, and the generated return current compensates the injected beam current (Zharkova 1997).

In a collisional model with Ohmic heating, return current energy losses in a fully ionised coronal plasma were shown to have a noticeable effect on the injected beam dynamics, particularly at the chromospheric level (Emslie 1980). Hence, the electron interaction with induced electric fields may govern the beam dynamics. As a result, less energetic electrons might not reach the deep chromosphere, but loose their energy in the lower corona (Aschwanden 2002).

The type of the excited electrostatic instabilities depends on the composition of beams and return-currents (Davidson 1983), i.e. on the ratio of their fluxes. The evolving unstable plasma waves can result in particle anomalous transport at the nonlinear stage. Assuming a collisional thick target model (Brown 1971), the spectrum obtained from the solar flare on 23 July 2002, for example, suggested an instantaneous electron flux of more than 2×10^{36} s^{-1} above 20 keV for 100 s (Holman et al. 2003). Taking the RHESSI source sizes, a conservative lower limit for the electron flux is 2.6×10^{18} cm^{-2} s^{-1}. For a beam speed of the order of 10^{10} cm s^{-1}, this implies a beam-electron number density of 2.6×10^{8} cm^{-3}. In all likelihood, the area is a factor of 5 to 10 lower, and the electron flux per unit area is 5–10 times higher (Fletcher 2005). This means that beam number density and the coronal background number density are, perhaps, comparable.

A stability analysis of a dilute beam plasma system ($10^{-4} < n_b/n_p < 10^{-1}$) of the excitation of Langmuir waves was carried out Rowland & Vlahos (1985). In the case of a higher beam density ($n_b/n_p \sim 0.2$) electron-acoustic waves become unstable (McQuillan & McClements 1988). The possible excitation of low-frequency ion-acoustic and ion-cyclotron waves by dense beams was studied (Cromwell et al. 1988). Numerical simulation studies have shown that ion-acoustic (Büchner & Elkina 2005) and electron-acoustic waves can heat the plasma. This causes an efficient dissipation of the electron flux through energy conversion.

Electron beam instabilities can lead to the development of electrostatic double layers (DLs) (Büchner & Elkina 2006). DLs are unique nonlinear electric field structures in free-energy supplied environments. An ideal DL consists of an unipolar electric field, i.e. it exhibits a monotonic potential drop, and the charge neutrality condition is violated locally (Langmuir 1929). Dynamically, however, DLs are formed by accumulating electron phase space holes which are characterized by bipolar electric fields (Block 1977). A sufficient condition for a DL structure is a net potential drop through the entire layer. For electrons with energies less than the first potential ramp, a DL provides an obstacle, which would stop the electrons at the ramp. The stagnation of the electron flow can dissipate the flow energy and heats the reflected electrons. In order to describe a basic feature of DLs, the local charge separation, a multifluid approach is required.

Double layers in current-free beam plasma, where a dense beam is neutralized by a return-current, are studied in the laboratory (Hairapetian & Stenzel 1990). Current-free DLs in solar coronal plasma were considered (Alfven & Carlqvist 1967; Khan 1989; Boswell et al. 2006). A combined action of anomalous resistivity and DLs was proposed to explain the dissipation of cosmic jets (Borovsky 1986). An analytical model of the diffusive acceleration of particles in auroral plasma due to interaction with weak double layers was developed (Lotko 1986). Auroral electron acceleration by double layers was considered (Borovsky 1992). Auroral acceleration requires multiple weak double layers, organized in a chain along the field lines, to form a sufficently large total potential drop. In general, double layers can effectively accelerate electrons and cause complicated nonlinear dynamics in the system, which has to be studied by means of numerical simulations.

A numerical study of DLs with semi-open boundary conditions was performed (Newman 2001). They intended to explain the ionosphere DC parallel electric field observed by the FAST (Fast Auroral SnapshoT) satellite (Lynch 2001). The dynamics of electron holes, created by an ion-acoustic instability, was discussed therein. The formation of DLs as a result of the nonlinear development of an electron current-driven instability was studied by means of a Vlasov code simulation (Büchner & Elkina 2006).

It is not yet known, however, through which mechanism DLs are created in a return-current beam-plasma system, which is typical for the solar coronal. The precise mechanism of energy conversion from bulk current kinetic energy to electrostatic wave energy and, at later stages, to electron and ion thermal energy via the interaction with DLs, is also unclear.

Our goal is to analyze the stability of a return-current beam plasma system in the solar corona and to investigate the consequences of the resulting wave-particle interaction, i.e. whether it might explain the broken-power-law electron spectrum retrieved from solar HXR observations.

In Sect. 2, we carry out a linear dispersion analysis for the most probable coronal parameters. To consider the nonlinear instability evolution, we performed a 1D Vlasov-code simulation and its spectral analysis. These results are presented in Sect. 3. At the nonlinear stage of the DL's evolution, fast electron holes are formed after electrons are accelerated by DLs. The dynamics of this unique phenomenon is discussed in Sect. 4, where we also discuss the heating of ions and electrons. To address the formulation of the broken-power-law spectra and the discrepancy of electron distributions retrieved from both footpoint- and coronal emissions, the dissipation and relative anomalous transport characteristics of electrons are discussed in Sect. 5.

A brief summary and a discussion of the implications of our results for the solar corona are given in Sect. 6.

2. Basic equations and linear dispersion analysis

A counter-streaming return-current beam plasma becomes unstable, and the generated waves dissipate the electron bulk motion, even though their net current is zero. To study the dispersion characteristics of this system a multifluid model is considered.

We assume a current and charge-neutrality system, i.e.

$$\sum_\alpha q_\alpha N_\alpha = 0 \qquad \sum_\alpha q_\alpha N_\alpha V_{d\alpha} = 0 \tag{1}$$

where N_α represents the densities of the beams, $V_{d\alpha}$ is the mean velocity in the beam flow direction and $v_{t\alpha}$ is the thermal velocity of the beam electrons. For collisionless plasma, large amplitude electrostatic waves have strong influence on the anomalous momentum transport property, hence the electrostatic condition ($\boldsymbol{b} = (c/\omega)\boldsymbol{k} \times \delta\boldsymbol{E} = 0$) is assumed, which indicates $\boldsymbol{k} \parallel \boldsymbol{E}$.

The dispersion relation of electrostatic linear perturbations in the return-current beam system is:

$$1 = \frac{\omega_{pi}^2}{\omega^2} + \frac{\omega_{p,Beam}^2}{\left(\omega_{*Beam}^2 - k^2 S_{Beam}^2\right)} + \frac{\omega_{p,RC}^2}{\left(\omega_{*RC}^2 - k^2 S_{RC}^2\right)}. \tag{2}$$

The Buneman mode (Buneman 1958) is a basic beam-plasma fluid-like instability (or ion-acoustic mode, IA, if thermal corrections are considered). In a return-current system, however, two electron populations exist. Their relative drift may also cause an electron-acoustic instability (Gary 1993).

To identify the different possible excitation mechanisms, we performed a sub-system dispersion analysis. In the beam-plasma system (without the third term on the righthand side of Eq. (2)) and the return-current beam plasma system (without the first term on the righthand side of Eq. (2)), the IA and the electron-electron two stream instability (EE) can be recognized via a detailed comparison of growth rates and dispersion characteristics. The EE coupling leads to a much higher growth rate if the real mass ratio is applied.

We solve the linear dispersion Eq. (2) for the parameters of solar coronal loops, with the real mass ratio ($m_i/m_e = 1836$) to find the dominant mode in the system. In Fig. 1, the growth rates along the directions of the beam and the return-current are shown as functions of density and temperature ratios. For isothermal beam and return-current ($T_{Beam}/T_{Plasma} \approx 1$), ion-acoustic mode is excited along the return-current direction and an EE two-stream instability in the beam direction. Beams ejected from the primary acceleration sites can, however, be heated along the path of propagation before interaction with the background plasma.

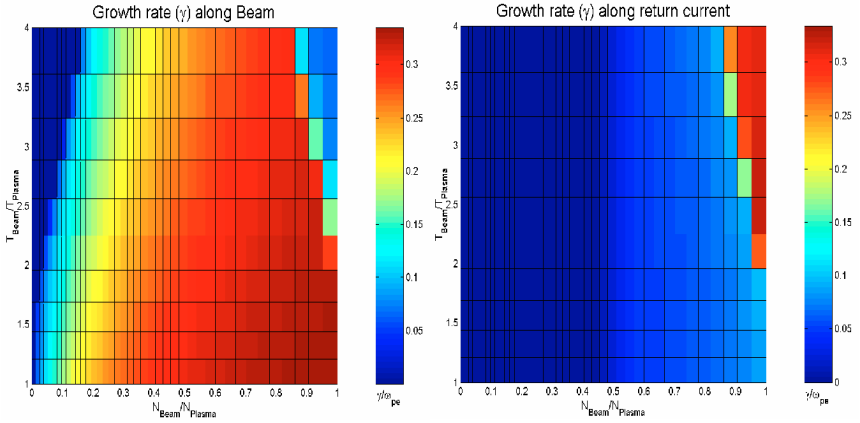

Fig. 1. The normalized largest growth rates of waves propagating along beam and return-current directions, shown as functions of density and temperature ratio for the real mass ratio of electrons and ions ($m_i/m_e = 1836$). Larger growth rates correspond to electron-electron acoustic (EE) mode while smaller growth rates correspond to the ion-acoustic (IA) mode.

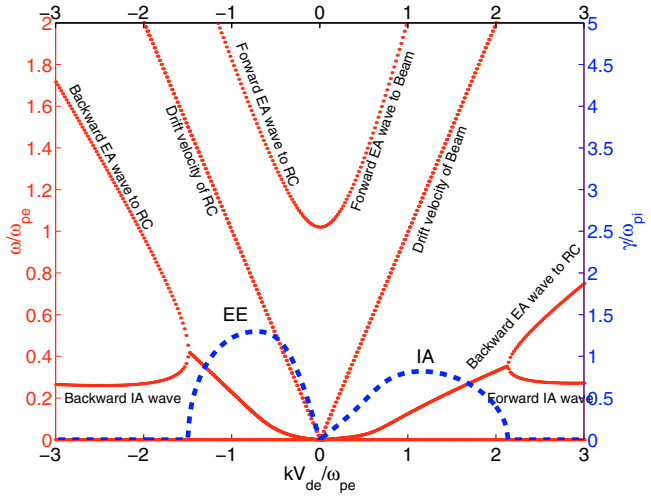

Fig. 2. Dispersion relations for $m_i/m_e = 25$. Wave frequencies (red dotted lines) and growth rates of unstable modes (blue dashed lines) in a warm return-current beam plasma are shown.

Hence, the dependence on the temperature ratio must also be studied.

For larger temperature ratios ($T_{\rm Beam}/T_{\rm Plasma} > 1$) and comparable electron densities of the beam and return-current ($N_{\rm Beam}/N_{\rm Plasma} \approx 1$), the IA and EE mode switch their propagation directions. The energy transport of Doppler-shifted electron acoustic waves of the beam and return current can be clarified by analyzing the coupling of the waves.

In order to compare with numerical simulation results, we carried out a linear dispersion analysis for a mass ratio ($m_i/m_e = 25$). The result with the reduced mass ratio is shown in Fig. 2. With the assumed electron temperature and current density of solar flares (Aschwanden 2006), the thermal velocity of electron $V_{te} \approx 2.58$ keV $= 5 \times 10^9$ cm s^{-1} and the bulk velocity of the beam is $V_{de} \approx c/3 = 1 \times 10^{10}$ cm s^{-1} (Kudriavtsev 1989; Fletcher 2005). During flares the beam temperature increases several times above that of the coronal plasma (Aschwanden 2006), hence we assume that the thermal velocity of the beam is twice the thermal velocity of the return-current:

$$\begin{aligned} V_{\rm d,Beam} &= -V_{\rm d,RC} = 2V_{\rm th,RC} \\ V_{\rm th,Beam} &= 2V_{\rm th,RC} = 2V_{\rm th,ion} \\ N_{\rm RC} &= N_{\rm Beam} = N_{\rm ion}/2. \end{aligned} \quad (3)$$

The dispersion analysis reveals two unstable waves modes (see Fig. 2). The wave frequencies are depicted by red dotted lines, and their growth rates are depicted by blue dashed lines. (Note that in our analysis the injected beam propagates in the positive direction.) An electron-acoustic wave propagates along the directions of the reverse current (negative K) due to an EE two-stream instability. The maximum growth rate $\gamma \simeq 1.5\omega_{\rm pi} \approx 1/3\omega_{\rm pe}$ is the characteristic growth rate of the resulting electron-electron two-stream instability, which is caused by a coupling of the forward propagating beam electron-acoustic wave and backward propagating return-current electron-acoustic wave.

Along the beam direction (positive K), an IA wave grows unstably due to a coupling between the backward propagating beam electron-acoustic wave and the forward propagating ion-acoustic wave, and the maximum growth rate is $\gamma \simeq \omega_{\rm pi}$.

The growth of unstable waves continues until the free energy of the system is reduced to marginal instability conditions. In order to study the resulting wave-particle interaction and the nonlinear evolution we use a fully kinetic 1D Vlasov code simulation.

3. Double layer formation and spectrum analysis

The evolution of an electron beam instability was investigated by means of a one-dimensional (1D) electrostatic Vlasov-Ampere code (Elkina & Büchner 2006). The code is based on an unsplit conservative finite-volume numerical discretization scheme, and it uses an open-boundary condition to study the evolution of the current-driven instability.

To study the nonlinear evolution of DLs in a current-neutralized beam plasma, we performed a simulation with the same parameters as used in dispersion analysis (Eq. (3)), i.e. a hot electron beam and an ambient cooler return-current electron drifting in the opposite direction to maintain the current neutrality condition. Both beams are modeled by drift-Maxwellian distributions. Ions form a stationary background at the beginning of the simulation with a Maxwellian distribution.

We use a moderate artificial mass ratio $m_i/m_e = 25$ to distinguish the difference in ion and electron motion. The assumption of an artifitially low mass ratio is necessary to allow the ions to respond within a reasonable simulation time. The length of the simulation domain is $3200\lambda_{\rm DE}$. With typical solar flare parameters, this corresponds approximately to ≃12 m in a 10^7 m flaring coronal loop (Aschwanden 2006). A periodic boundary condition is a reasonable and sufficient assumption for a such long system.

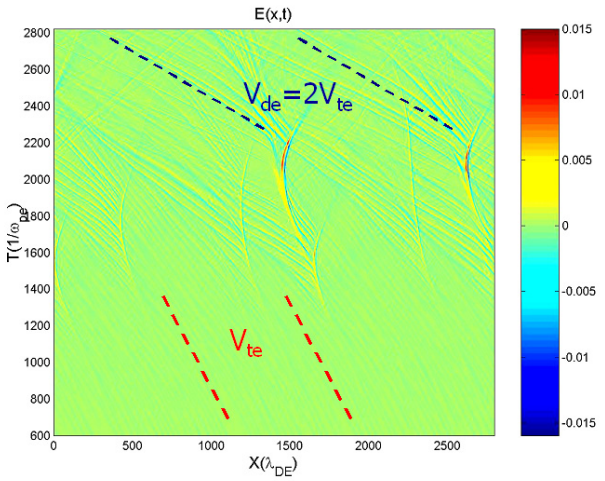

Fig. 3. Electric field history $E_x(x,t)$. Double layers appear at $T\omega_{pe}^{-1} = 1400$. Two pronounced phase velocities are (1) the original electron-acoustic waves velocity V_{te}, and (2) the velocity of fast electron holes $V_{de} = 2V_{te}$.

DLs can be created at the nonlinear stage if the Bohm condition (Bohm 1949) is satisfied, i.e.

$$j_c = ne\sqrt{2kT_e/m_e} \tag{4}$$

which is satisfied for the solar flare plasma parameters used in our simulation setup (Eq. (3)).

The simulation is performed until ($T = 2800\omega_{pe}^{-1}$), which allows one to investigate the complete evolution of DLs. The spatial-temporal evolution of the electric field is shown in Fig. 3. During the linear stage ($T \leq 700\omega_{pe}^{-1}$) the electron-acoustic waves (EE-mode) appear first in accordance with the linear stability prediction (see Fig. 2), and propagate along the return-current direction.

The nonlinear stage of the instability is characterized by the apperance of double layers. As one can see in Fig. 3, multiple double layers are created and later dissipated. Their life-time is about $T_{life} \sim 800\,\omega_{pe}^{-1}$. All double layers initially, i.e. during the first half of their life-time, move in the direction of the return-current electron flow. In the second half of their life-time DLs change their direction and start to move in the beam direction. A similar behaviour of double layers was observed in two-ion population plasma used to simulate auroral weak double layers (Yajima & Machida 2001).

The characteristics of unstable waves and nonlinear structures, their frequencies and wave numbers, can be obtained via a spectral analysis of the generated electric field for different time intervals.

Figure 4 depicts the spectra for the simulation intervals (1) T:$700\omega_{pe}^{-1}$; (2) T:$1400\omega_{pe}^{-1}$ and (3) T:$2800\omega_{pe}^{-1}$. The color-coding indicates the spectral intensity of the modes

$$A(k,\omega) = \sum_{n=0}^{N-1}\left(\sum_{s=0}^{M-1} a(x,t)\mathrm{e}^{\frac{-2\pi i}{M}s\omega}\right)\mathrm{e}^{\frac{-2\pi i}{N}sk}. \tag{5}$$

The wave frequencies obtained by the linear dispersion analysis are superposed (red curves) in Fig. 4. At the linear stage (1) one can see that the first excited wave is propagating in the direction of the return-current (negative $\boldsymbol{K}$). This agrees with the prediction of the linear theory that the EE mode grows faster. The second period (2) corresponds to the appearance of DLs. The excited wave spectrum is broader both in wave numbers and in frequency. Note that the phase-velocity of unstable waves increases but does not reach the drift velocity.

Before stage (3) DLs start to decay and, consequently, the fast electron holes generated by the double layers take over the global dynamics of the simulation in this third phase, as products of the interaction with DLs.

4. Dynamics of fast electron holes

A real DL consists of several asymmetric bipolar electric field structures, which all together cause a net potential drop. DLs primarily affect electrons in two ways: (1) as the phase space structures shown in Fig. 5 near $X = 20(c/\omega_{pe})$ and $X = 8(c/\omega_{pe})$, the first potential dip on the positive side of DL stops low-energy electrons since electrons are accelerated toward the higher potential side; (2) the overall potential difference accelerates those electrons that are able to cross the first barrier.

Contrary to the initial electron-acoustic waves (EE) generated by the interaction of beam and return-current electrons at the linear stage, fast electron holes result from a secondary electron two-stream instability via the interaction of DL-accelerated return-current electrons with the background low speed return-current electrons. In the simulation interval shown in Fig. 5, the generation of fast electron holes is in the intervals $X = 15{-}18(c/\omega_{pe})$ and $X = 5{-}7(c/\omega_{pe})$.

The additional third electron beam is created by the DL, with its own characteristic drift and thermal velocities. To analyze the fast electron holes triggered by the third electron beam, we performed a sub-system dispersion analysis in which the thermal spread and drift difference of DL-accelerated return-current electrons and the background low speed return-current electrons are considered. The rough estimate of the resulting secondary two-stream instability caused by the third beam shows that the electron holes should propagate at a speed of ($V_{Holes} = 2V_{te} = V_{de}$) to the background ions. This explains the observed phase velocity of the fast electron holes.

5. Plasma heating and anomalous transport

The energy transfer is always an attractive topic in solar coronal studies. During flares, evolution of the plasma distribution takes place in the beam precipitation from the upper corona to the chromosphere. The question to be addressed is: can the broken-power-law spectrum be explained by the energy and momentum transfer due to the excitation of DLs?

Consider both the energy range of hard X-ray emissions (≥5 keV) and soft X-ray emissions (<5 keV). The HXR are mostly generated via thick-target bremsstrahlung while soft X-rays (SXR) result from free-free electron scattering. Bright emissions of SXR and extreme ultraviolet (EUV) radiations are a consequence of plasma heating in coronal loops. Coronal HXR emissions correspond to low photon energies (<30 keV), and their characteristics are consistent with the radiation from a hot quasi-thermal plasma. Instead the chromospheric "footpoint" emission is thought to be generated by vast numbers of non-thermal particles accelerated during a flare.

Let us further assume that the electrons are beamed from the primary acceleration sites at the topside of coronal loops, and that the electron spectra are primarily nonthermal (Antonucci et al. 1995); the observed coronal thermal emission in the collisionless coronal plasma should be generated through dissipation of the original nonthermal electron beam.

The simulated evolution of the space-averaged distributions of beam electrons and of the return-current electrons is depicted

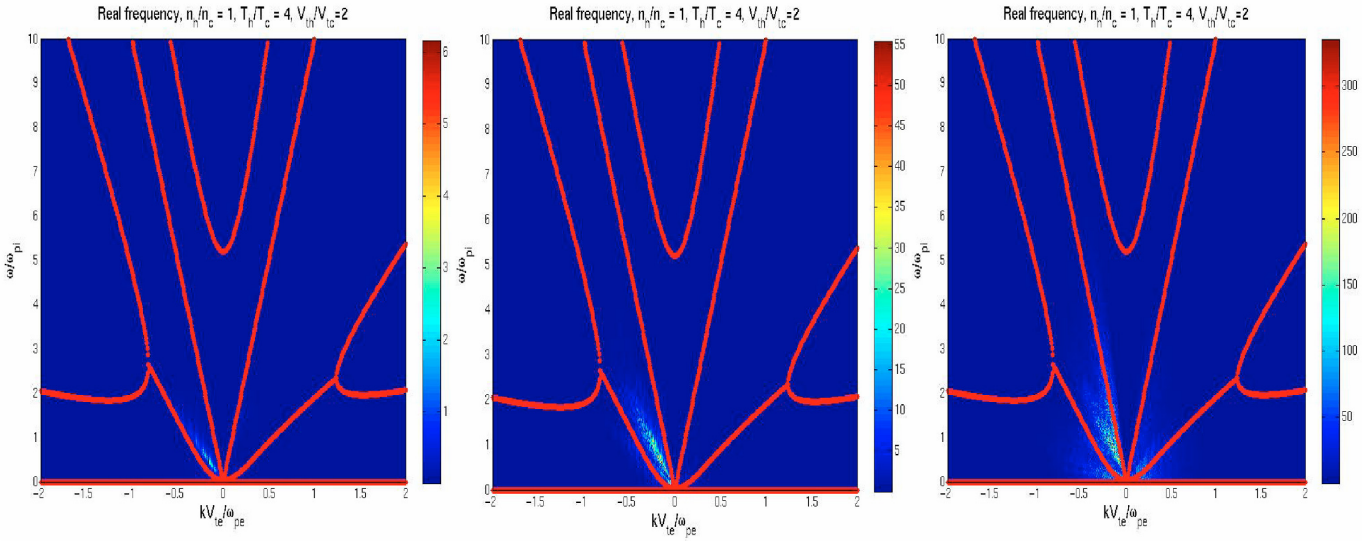

Fig. 4. The spectra of simulation at different times are shown in each panel, 1) T:0–$700\omega_{pe}^{-1}$ 2) T:0–$1400\omega_{pe}^{-1}$ 3) T:0–$2800\omega_{pe}^{-1}$. The color-coded indices show the 2D FFT transform coefficient. In the nonlinear stage fast electron holes appear, and propagate at velocity of return-current drift $2V_{te} = V_{de}$

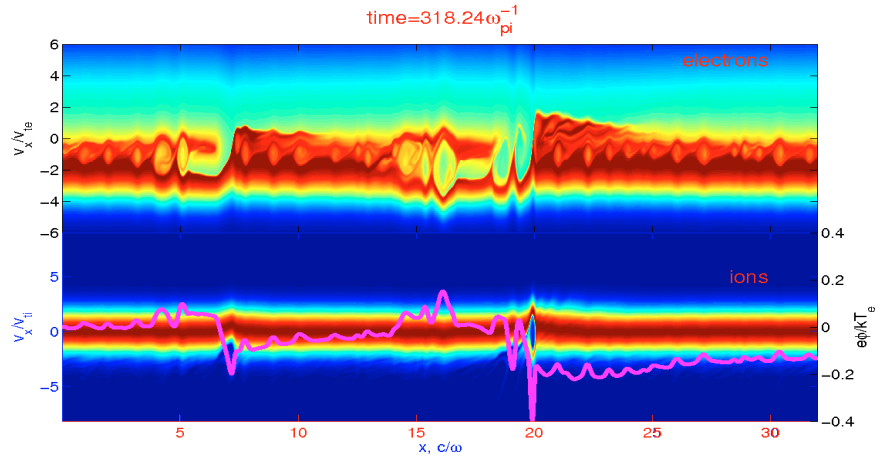

Fig. 5. Electron and ion phase spaces are given at time $T = 318\omega_{pi}^{-1} = 1590\omega_{pe}^{-1}$. Electric field potential $e\phi/k_B T_e$ normalized by electron temperature is shown by the solid line.

in Fig. 6. One can see the space-averaged distribution of the original non-thermal beam ($V_{de} > V_{te}$) exhibits heating after the appearance of DLs at $T = 1400\omega_{pe}^{-1} = 280\omega_{pi}^{-1}$. A similar behavior is observed in the space-averaged distribution of the return-current, which can be seen in the lower panel of Fig. 6. As one can see in the figure, DLs can inhibit the bulk motion of electrons. This is not the behavior of ideal DLs that consist only of a potential drop. The separate plots of beam and return-current electron distributions show that the direct beam- and return-currents are enormously slowed down, while the non-thermal distribution is broadening. This affects mostly the lower energy part of electrons, which contribute rather to the generation of SXT and coronal HXR. Another interesting point to notice is that the higher energy part of the direct beam is not influenced very much, which might explain the nonthermal chromospheric HXR sources. Note that in (Zharkova 1997) a similar conclusion is given, that the return-current mainly results in electron density depletion and the spectrum flattening at the low energy part, using their CEM model (Collisional, Electric and converging Magnetic field).

Considering their effects on electrons, we suggest that DLs play a role as an energy converter that transfers the original bulk energy of a beam into thermal energy. The same effect is true for the return-current. After DLs have transformed the electron drift energy into thermal energy, they gradually fade away. The reason is that the acceleration of fast electron holes takes away electric field energy. DLs disappear when free beam energy drops to the marginal threshold of any instability. In Fig. 6 the averaged electron motion of individual species, their currents, are shown as black solid lines. The heavier background ions are also thermalized.

To understand the observed HXR broken-power-law spectrum, we look at the combined space-averaged distribution of beam and return-current. As one can see in Fig. 7, a considerable number of return current electrons are dragged along by the beam toward the positive propagation direction after the appearance of DLs ($T = 421\omega_{pi}^{-1}$). This results in a total density increase of the downward-propagating electrons (positive V_x), especially in the low energy range. The right panel of Fig. 7 shows the space-averaged distribution at simulation time $T = 421\omega_{pi}^{-1}$

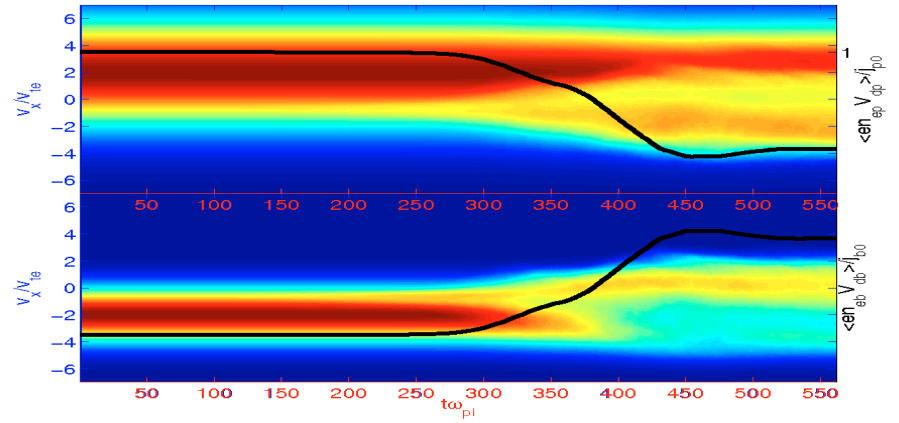

Fig. 6. Spatially averaged electron distribution function corresponding to beam and plasma. Averaged current contribution are shown by continious line.

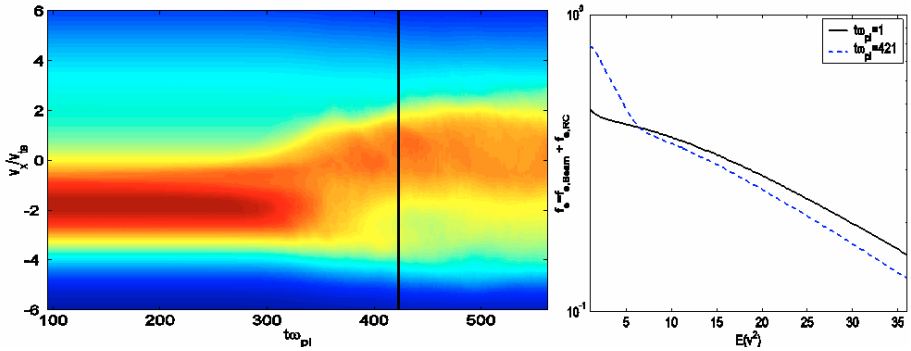

Fig. 7. Combined spatially-averaged electron distribution function of beam and return current. For the right panel, the space-averaged downward-propagating ($V_x \geq 0$) distribution function at ($T = 421\omega_{pi}^{-1}$) is shown as a blue dashed line, while the initial distribution is shown as a black solid line.

as a blue dashed line, compared with the initial distribution as a black solid line, the downward-propagating electron (positive V_x) in the low energy range has a higher density than that in the higher energy range. The result shown in the right panel of Fig. 7 is clearly a broken-power-law spectrum.

The plasma environment we simulated here is the quasi-homogeneous part of the coronal loop above the transition region. Below the transition region the plasma density has strong density gradient. The impact cross section depends on the background plasma density, and the incoming electrons, with different drift energy, should cause emission peaks at different altitudes in the chromosphere, as shown in Fig. 4 of (Aschwanden 2002). If this electron beam created at the late stage of the nonlinear beam evolution can further travel down to the chromosphere by maintaining these distribution characteristics, it will eventually radiate HXR through collisional Bremsstrahlung. Since the downward-propagating electron is dense in the low energy part, two indices are required for the drift-Maxwellian distribution fitting, thus revealing a broken-power-law energy spectrum.

6. Discussion and conclusion

In order to understand the evolution of the electron spectrum in the solar corona we have investigated the interaction of a precipitating beam of energetic electrons with its self-generated return current. For this purpose we have carried out a linear instability analysis and a one-dimensional Vlasov code simulation of a return-current beam plasma system for typical coronal parameters.

In previous studies, instabilities in beam-current systems were usually considered to be the ion-acoustic type (Watt et al. 2002; Büchner & Elkina 2006). This is the case of only one electron beam in the system. An energetic electron beam in the corona will, however, induce an oppositely directed return current flow that maintains the current-free condition. Our sub-system dispersion analysis, applied to coronal plasma parameters, shows that forward and backward unstable waves are generated from different origins. In addition to an ion-acoustic instability along the original electron beam direction, an electron-acoustic two-stream instability is excited along the return-current direction. The latter has a larger growth rate and dominates the linear stage.

To consider the nonlinear instability evolution and wave-particle interaction of the saturated state, a Vlasov code simulation was performed. We found that multiple double layers develop in the system. Spectrum analysis of the generated electric field allowed us to analyze the evolution of the nonlinear structures out of the linear instability phase, the so called double layers (DLs).

After the appearance of DLs, fast electron holes also appear due to electron acceleration by the DLs. As products of DLs, these fast electron holes propagate at the drift velocity of the return-current. The phase velocity estimate from dispersion analysis and from the spectrum analysis shows that the fast electron holes result from a secondary electron two-stream instability, which is generated by the self-interacting return-current electron beams. The unique generation mechanism of this nonlinear dynamical phenomenon has not been reported in the previous study of beam and return-current system. We conclude that in a

current-free return-beam coronal plasma, fast electron holes are generated from a secondary two-stream instability.

Note that this mechanism would also appply to the observed topside ionosphere fast electron holes if the plasma comprises a drifting beam and background ions. Indeed, space plasma observations of the FAST (Fast Auroral SnapshoT) satellite have discovered a variety of nonlinear localized electric field structures in the auroral ionosphere. Isolated bipolar field structures have been observed in the downward current region where they have been interpreted in terms of electron phase-space holes moving upward at speeds in the order of electron drift velocities (Ergun 1998). Our analysis has revealed a similar behavior of fast electron holes for the solar coronal condition at the late stage of evolution, which propagate at the drift speed of the return-current.

Our results can explain the deduced electron beam density of the chromospheric footpoints (Fletcher 2005) and the commonly observed broken-power-law HXR spectrum of the solar corona.

Since the return-current is a reasonable assumption in coronal loops, because the ejected electron beam propagates through a fully ionized plasma, DLs are expected to generate and influence the electron transport in the beam and return-current system. As shown in the individual space-averaged distribution of beam and return-current electrons, we found that higher energy beam electrons are not influenced very much, but lower energy beam electrons are. The kinetic energy of the slowed-down beam electrons changes the electron propagation direction of return-current. As a consequence, the combined electron distribution clearly exhibits a density increment of downward-propagating electrons (positive V_x). Hence, we suggest that the observed broken-power-law spectrum is a natural consequence of the interaction of beam electrons with the self-generated current-free DLs.

Acknowledgements. The authors thank L. Fletcher for discussion of the HXR observation of energetic solar electron beams. K.-W. Lee gratefully acknowleges the support from the DAAD-NSC grant (No. 95 -2911-I-008-008-2). N. Elkina acknowledges her support by the DFG (project EL 488/1-1).

References

Alfven, H., & Carlqvist, P. 1967, Sol. Phys., 1, 220
Antonucci, E., Dodero, M. A., Somov, B. V., & Verneta, A. I. 1995, Il Nuovo Cimento D, 17, 1149
Aschwanden, M., Fletcher, L., Sakao, T., Kosugi, T., & Hudson, H. 1999, APJ, 517, 977
Aschwanden, M. 2002, Sol. Phys., 210, 383
Aschwanden, M. 2006, Physics of the solar corona (Springer)
Block, L. 1977, Ap&SS, 55, 59
Bohm, D. 1949, Minimum ionic kinetic energy for a stable sheath (New York: McGraw-Hill)
Borovsky, J. 1986, ApJ, 306, 451
Borovsky, J. E. 1992, Phys. Rev. Lett., 69, 1054
Boswell, R. W., Marsch, E., & Charles, C. 2006, ApJ, 640, L199
Brown 1971, Sol. Phys., 18, 489
Büchner, J., & Elkina, N. 2005, Space Sci. Rev., 121, 237
Büchner, J., & Elkina, N. 2006, Phys. Plasmas, 13, 2304
Buneman, O. 1958, Phys. Rev. Lett., 1, 119
Cromwell, D., McQuillan, P., & Brown, J. C. 1988, Sol. Phys., 115, 289
Davidson, R. 1983, Basic Plasma Physics 1: Chap. 3.3 Kinetic waves and instabilities in a uniform plasmas (North-Holland Publishing Company)
Newman, D. L., Goldman, M. V., Ergun, R. E., & Mangeney, A. 2001, Phys. Rev. Lett., 87, 255001
Elkina, N., & Büchner, J. 2006, J. Comp. Phys., 14
Emslie 1980, ApJ, 235, 1055
Ergun 1998, Geophys. Rev. Lett., 25, 2041
Fletcher, L. 2005, Space Sci. Rev., 121, 141
Gary, S. P. 1993, Theory of Space Plasma Microinstabilities ed. S. P. Gary (Cambridge, UK: Cambridge University Press), 193
Hairapetian, G., & Stenzel, R. 1990, Phys. Rev. Lett., 65, 175
Holman, G. D., Sui, L., Schwartz, R. A., & Emslie, A. G. 2003, ApJ, 595, L97
Khan, J. 1989, PAJA, 8, 29
Kudriavtsev, I. V., & Charikov, I. E. 1989, Pis'ma v Astronomicheskii Zhurnal, 15, 353
Langmuir 1929, Phys. Rev., 33, 954
Lotko, W. 1986, J. Geophys. Res., 91, 191
Lynch, K. A., & Bonnell, J. C. C. W. P. W. J. 2001, Am. Geophys. Union, Spring Meet. 2001, SM41B-04
MacKinnon, A. L., B. J. H. J. 1985, Sol. Phys., 99, 231
McQuillan, P., & McClements, K. G. 1988, J. Plasma Phys., 40, 493
Rowland, H. L., & Vlahos, L. 1985, A&A, 142, 219
Watt, C. E. J., Horne, R. B., & Freeman, M. P. 2002, Geophys. Rev. Lett., 29, 4
Yajima, A., & Machida, S. 2001, Earth, Planets and Space, 53, 139
Zharkova 1997, A&A, 320, 13